Review of Scientific Instruments

Development of a 3-D visible limiter imaging system for the HSX stellarator

Cite as: Rev. Sci. Instrum. **88**, 123508 (2017); https://doi.org/10.1063/1.5000855
Submitted: 18 August 2017 . Accepted: 05 December 2017 . Published Online: 22 December 2017

C. Buelo, L. Stephey, F. S. B. Anderson, D. Eisert, and D. T. Anderson

AIP Publishing

Development of a 3-D visible limiter imaging system for the HSX stellarator

C. Buelo,[a] L. Stephey, F. S. B. Anderson, D. Eisert, and D. T. Anderson
University of Wisconsin–Madison, Madison, Wisconsin 53706, USA

(Received 18 August 2017; accepted 5 December 2017; published online 22 December 2017)

A visible camera diagnostic has been developed to study the Helically Symmetric eXperiment (HSX) limiter plasma interaction. A straight line view from the camera location to the limiter was not possible due to the complex 3D stellarator geometry of HSX, so it was necessary to insert a mirror/lens system into the plasma edge. A custom support structure for this optical system tailored to the HSX geometry was designed and installed. This system holds the optics tube assembly at the required angle for the desired view to both minimize system stress and facilitate robust and repeatable camera positioning. The camera system has been absolutely calibrated and using H_α and C-III filters can provide hydrogen and carbon photon fluxes, which through an S/XB coefficient can be converted into particle fluxes. The resulting measurements have been used to obtain the characteristic penetration length of hydrogen and C-III species. The hydrogen λ_{iz} value shows reasonable agreement with the value predicted by a 1D penetration length calculation. *Published by AIP Publishing.* https://doi.org/10.1063/1.5000855

I. INTRODUCTION AND BACKGROUND

The Helically Symmetric eXperiment (HSX) is a quasisymmetric stellarator. It was designed in such a way as to fully exploit 3D flexibility to achieve a magnetic field with advantageous properties. While this highly shaped 3D design was shown to achieve its goal of reducing neoclassical particle losses,[1] it also presents practical challenges in diagnostic design and measurement access. Making measurements of core plasma quantities in this 3D environment can be difficult, and as a result of spatially varying edge magnetic structure, flux tubes, and heat and particle fluxes, measurements of 3D edge quantities can be particularly challenging.

Because HSX has a four-fold symmetry, it has four large corner ports typically referred to as boxports. At the top and bottom of one boxport, HSX has two carbon limiter structures which can be inserted and removed to change edge properties. One of these boxports with the limiter structure can be seen in Fig. 1. Because of the positioning of these limiters, there are currently no HSX ports which can provide a direct line of sight to the limiters. Therefore, a mirror and lens optical assembly was necessary to obtain an approximately perpendicular view of the top limiter. The mirror at the end of this assembly must extend approximately 1-2 cm inside the vessel into the edge plasma to provide the necessary view.

A parallel view of the HSX limiter could in principle be possible with a system viewing the limiter from above. However, the additional information provided by the perpendicular view will allow substantially more edge physics results to be obtained. One result included in this paper is λ_{iz}, the radial particle penetration length of both doubly ionized carbon (from C-III emission) and neutral hydrogen (from H_α emission). Another result this diagnostic can provide is the integrated carbon and hydrogen particle flux to the limiter (within the camera line of sight). Additionally, this diagnostic can also provide the 2D limiter carbon and hydrogen particle flux footprint on the limiter. This spatially resolved footprint, through comparison to both magnetic field line following calculations and also to more sophisticated fluid-kinetic plasma simulations (including EMC3-EIRENE[2]), can provide estimates of the HSX edge particle diffusivity, $D_\perp$.[3,4] Using the data obtained from this diagnostic, these studies will be performed as future work.

A similar optical system, i.e., the lens and mirror tube, was previously used as a gas-puff imaging diagnostic to study TEXTOR edge turbulence.[5] The details of its lens and mirror components can be found in the study of Shesterikov *et al.*[6] This optical system is depicted in Fig. 2 and consists of a long stainless steel tube with a polished stainless mirror tilted to 60° at the end with a system of lenses at the top. This paper will go over the design process of the supports, the diagnostic setup of the camera, and the preliminary results from the system.

II. NEW SUPPORT SYSTEM DESIGN

The 3D modeling software (Autodesk Inventor) played a major role in the design of this system. The HSX vessel geometry, coil geometry, and port geometry as well as a need for post-installation adjustment had to be taken into account in order to design this complex system in a relatively constrained space as illustrated in Fig. 3.

The final design that satisfied these constraints is shown in Fig. 4. This support system is comprised of a 6 in. stainless steel vacuum flange welded to three stainless steel support arms and a stabilizing ring. The 6 in. flange in this case is used only to join the support structure to another vacuum flange; the underside bolt holes were enlarged to accommodate the nuts for this connection. This additional flange is what allows the system to be independent of the vacuum connection. The flange was cut in two pieces as indicated in Fig. 4 to enable the assembly to be constructed in pieces around the optical system. This design choice also increased the strength of the system by decreasing the required length of the support arms.

In what follows, we will now describe the design philosophy and process. Before it was removed from HSX, the

[a]Electronic mail: cjbuelo@wisc.edu

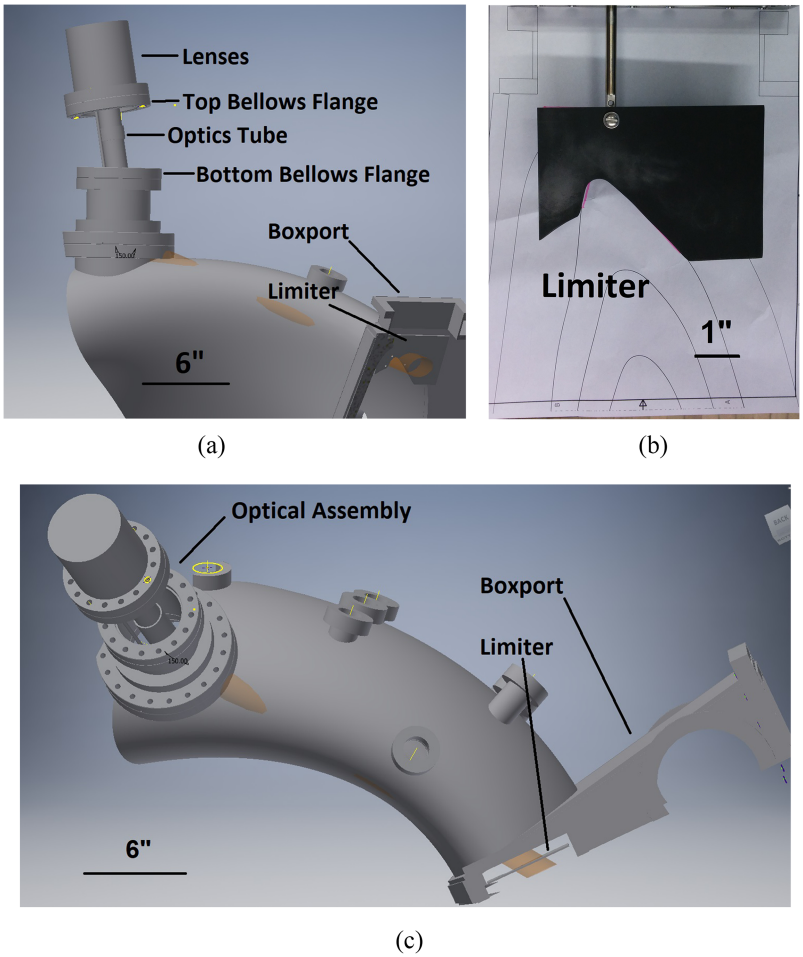

FIG. 1. (a) Autodesk Inventor rendering of the limiter-viewing optics and boxport with the limiter. The camera position is directly above the lenses, and the camera viewing cone is shown in orange, and portions of the cone that intersect with the HSX vacuum vessel can be seen. (b) One of the two HSX graphite limiters, inserted at the top of the boxport. The micrometer stage allows the limiter to be incrementally inserted and removed. LCFS in the figure stands for the last closed flux surface, separating the core from the edge, which the limiter is designed to follow. (c) Overhead view of the limiter-viewing optics and boxport showing geometry required to view the limiter.

location of several points on the previous support structure was measured. These points were then reproduced in the 3D modeling workspace, allowing the viewing plane of the previous support system to be reconstructed. The angle between the plane of the bottom of the bellows and the optics tube plane was determined to be 10.07°. The accuracy of the angle is needed to within a few tenths of a degree to achieve the proper viewing angle, calculated by using the small angle approximation. The optics flange was then constrained to be flat against this plane, and the optics tube was centered in the opening of the base.

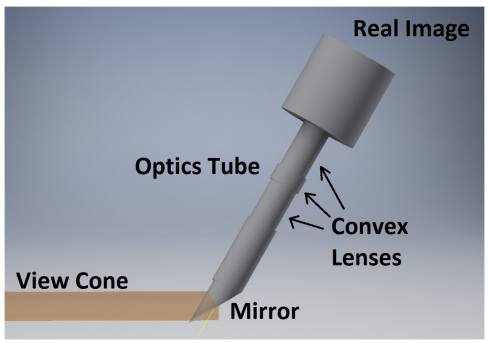

FIG. 2. The mirror/lens assembly as modeled in AutoCAD Inventor. The 60° mirror is seen at the bottom of the assembly. This is the portion of the assembly that is inserted and retracted to shield the mirror. More information about the mirror/lens assembly can be found in the study of Shesterikov *et al.*[6]

The three arms were designed so as to hold the optical system at the necessary angle to obtain a view of the limiter, roughly a third of a revolution away from each other. This angle can be seen in Fig. 4. This design resulted in two identical arms that support the assembly from behind, and one different arm that supports the assembly from the front. The arms were shaped so as to avoid contact with the relatively fragile bellows. To reduce stress on the system, the optical system can only be inserted or retracted in this plane, i.e., the system is always at a constant angle relative to the HSX vacuum vessel, and no bending of components is required. In addition, the fixed angle established with the support arms allows the camera/optics position to be stable and reproducible.

Three threaded rods join the arms to the optical system. Manual adjustment of nuts on these threaded rods is used to raise or lower the optical system to the desired position relative to the support structure. Surrounding the optics tube are the vacuum bellows, which expand and contract as the optical system travels up and down.

After installation of the supports, the final vacuum connection to be made was the connection to the HSX vessel. This was deliberately chosen as it is a rotatable connection which allows manual adjustments to the system to correct for any differences between the modeled and

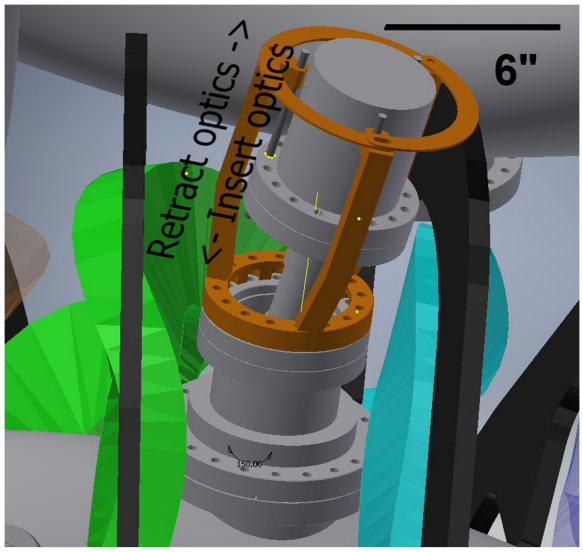

(a)

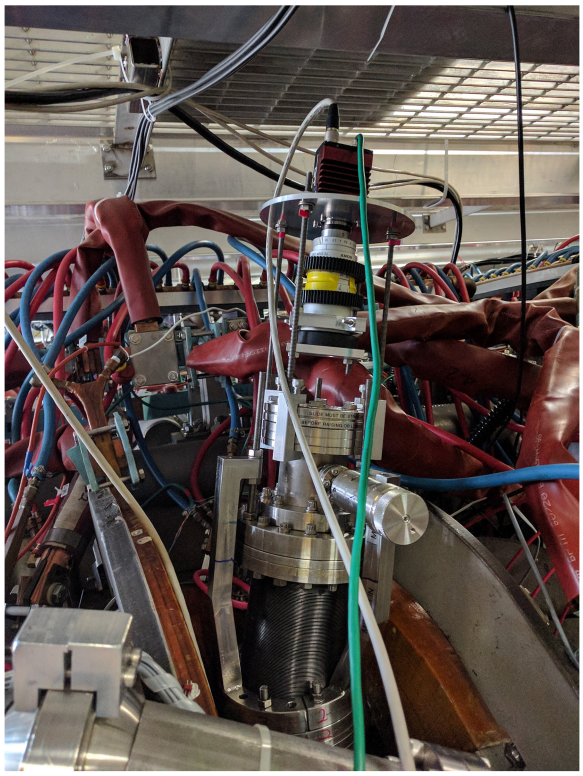

(b)

FIG. 3. (a) Final 3D model of the optics tube and support assembly with the three-part support ring on top. The support assembly is shown in orange, machine coils are in blue and green, and the coil supports are in black. The three threaded rods can be seen joining the support structure and the optics assembly. The adjustment nuts would be attached to the top of the threaded rods above the arms. (b) Optics tube and new support assembly without the support ring and camera with lens installed on the vessel.

as-built geometry. The optics tube was lowered into the position, and the limiter target was inserted at the LCFS and illuminated with flashlights. The support system was then rotated while monitoring the camera image. When the limiter image was appropriately centered in the camera frame,

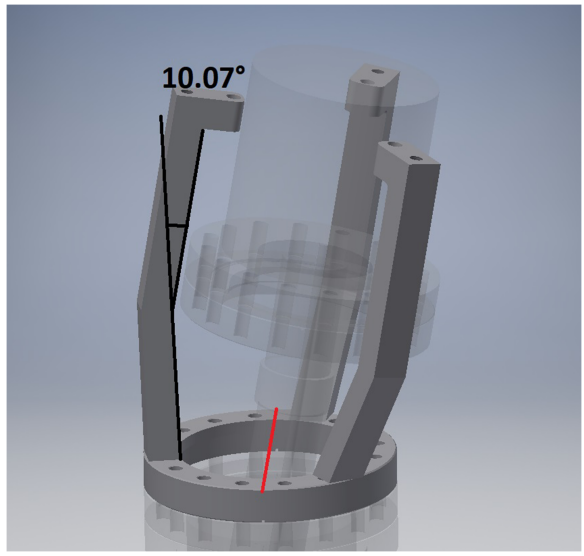

FIG. 4. The final stainless steel support system design. The three arms are welded to the flange at the base. The flange is cut in half as delineated by the red line to enable the assembly to occur around the optical components. The angle required to obtain the limiter view is noted.

the final vacuum connection was secured, effectively freezing the support in place. The design of these supports and installation procedure were chosen to allow *in situ* alignment of the entire system with enough degrees of freedom to ensure proper alignment of the camera before finishing the vacuum seal.

III. DIAGNOSTIC CAMERA CONFIGURATION

The visible camera is a Prosilica GT1290, triggerable, 1.2MP, 14 bit mono camera with 1280 × 960 resolution and digital exposure and gain control. With its current triggering scheme, it captures a single frame per plasma shot, but in principle this can be changed to capture several frames per discharge if additional triggers are provided, the image height is reduced, and the photon flux is sufficiently large. This will constitute future work. In addition, possible future upgrades to this system could include changing the optics tube lenses to a material transparent to IR, which would allow the camera to make heat flux measurements since the camera CCD is sensitive to the near IR (700-1000 nm). A dedicated infrared camera could also be used.

The camera lens is a Sony TV zoom 1:1.8 12-75 mm C mount lens with adjustable zoom, focus, and iris settings. It allows for a pixel resolution on the order of 0.02 cm/pixel. The effects of chromatic aberration result in different focal lengths (1-2 mm difference) for the H_α (656.28 nm) and C-III (465.03 nm) filters. This is accounted for by changing the focus of the camera between pre-calibrated positions for the different filters. If not accounted for, this results in blurring on the order of a few mm, enough to significantly impact the quality of measurement of quantities such as the ionization length. The camera is attached to the optics tube via an adjustable custom mount, allowing it to be moved along the axis of the optical system. A custom filter holder positions a

single filter in front of the camera lens. If necessary, the filter can be easily interchanged.

The camera system has been absolutely calibrated to determine H_α and C-III photon flux. This end-to-end calibration was performed using an integrating sphere using several exposure and gain settings. Using the manufacturer provided filter transmission curve information, the sphere and filter information was convolved to determine the total expected transmission. Assuming paraxial propagation, the image obtained for each exposure and gain setting was used to determine an image intensity-to-photon-flux calibration factor. This resulted in a 2D lookup table of calibration factors as a function of exposure time and gain settings for each filter.

It is important to note that the conversion between a photon flux and a particle flux requires an S/XB coefficient which equates the number of measured photons to the number of ionizations which resulted in the photon emission.[7] The S/XB coefficient is defined as the ratio of the collisional ionization coefficient, S, to the product of the branching ratio, B, and the excitation rate coefficient, X. Both of these ratios are well-known for the H_α and C-III lines used in this work.

Using this method, the number of ionizations can be related to a particle flux under the assumption that the particles are either ionized or dissociated within the line of sight of the camera.[7] The S/XB coefficient depends on both the local plasma temperature and density, and therefore this information must be known either from measurements or from modeling. The details of this commonly used method are described in Pospieszczyk,[7] Hintz and Bogen,[8] and Brezinsek *et al.*[9]

IV. EXPERIMENTAL RESULTS

Approximately 60 images were obtained in the HSX Quasi-Helically Symmetric (QHS) configuration, which is the configuration for which the limiter geometry was designed. The hydrogen plasma was heated with 50 kW of Electron Cyclotron Resonance Heating (ECRH) power, resulting in core temperatures around 1 KeV and core densities of $4\text{-}6 \times 10^{18}$ m^{-3}. Both H_α and C-III filters were used to measure photon fluxes. The CCD exposure times for the H_α and C-III images were 2 ms and 40 ms, respectively, due to the relative differences in photon intensity for each emission line.

Representative images of the H_α and C-III photon fluxes are shown in Figs. 5 and 6, respectively. Conversion into real space coordinates was done using the relative rotation of the limiter using the 3D model shown in Fig. 1, and the known dimensions of the limiter to determine the pixel resolution. The C-III and H_α ionization lengths were obtained by fitting an exponential to the image intensity off of the inner limiter edge as described in Figs. 5 and 6.

A single-term exponential fitting was used in order to determine the particle penetration length, λ_{iz}, for both hydrogen and C-III. The results from these exponential fits are displayed on the plots in Figs. 5 and 6 and indicate that the hydrogen penetration length is approximately 12 ± 1.02 cm, and the C-III penetration length is approximately 4.8 ± 0.3 cm. The uncertainties in these values of λ_{iz} are the sum in quadrature of a geometrical uncertainty factor (6.2%) and the error in the 95% confidence exponential fitting.

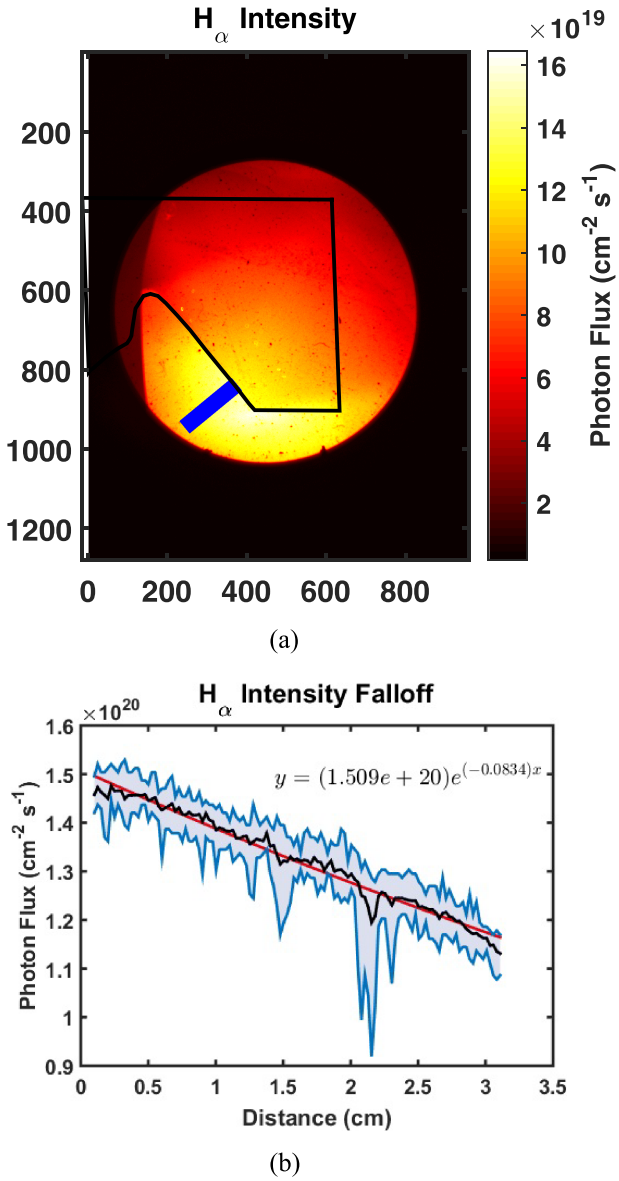

FIG. 5. (a) One data shot of H_α limiter photon flux data with the limiter outline in black. Axes scale in pixels. (b) Mean photon flux data (black line) obtained averaging the 11 offset, parallel image profiles spanning the blue rectangle. This averaging was done to improve statistics and reduce the effects of CCD noise and mirror dust. The corresponding exponential fit (red line) and the equation of this fit, from which λ_{iz} was determined, are also specified on the plot. The top and bottom of the error regions are taken from the max and min values at each position along the 11 profiles, respectively.

As a check, we can compare the λ_{iz} value obtained for hydrogen to the prediction from a 1D slab calculation,[10]

$$\lambda_{iz} = \frac{v_n}{n_e \langle \sigma_{ion} v_e \rangle}, \tag{1}$$

where v_n is the thermal velocity of the neutral particle (assumed to be room temperature, 0.026 eV), n_e is the plasma density, and $\langle \sigma_{ion} v_e \rangle$ is the rate coefficient for the dominant ionization process (electron impact ionization). We perform this calculation for molecular hydrogen only because in the HSX operational density range, we expect that the atomic hydrogen has a mean free path on the order of the HSX device size.[11] For this reason, resolving λ_{iz} for atomic hydrogen with this

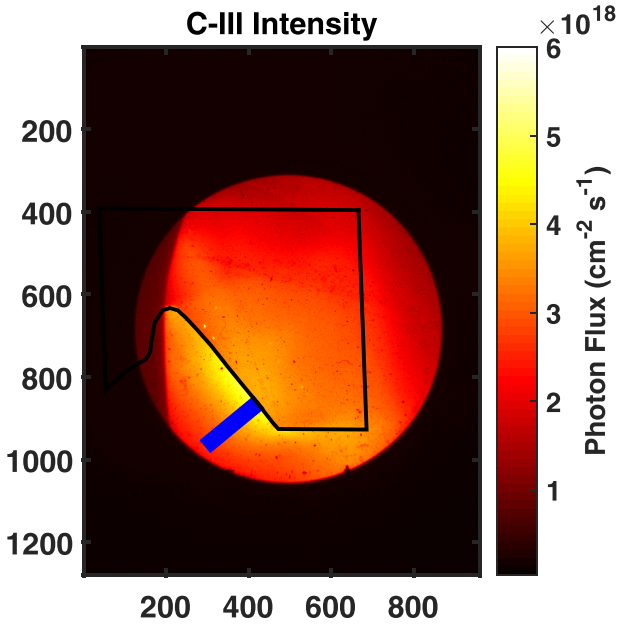

(a)

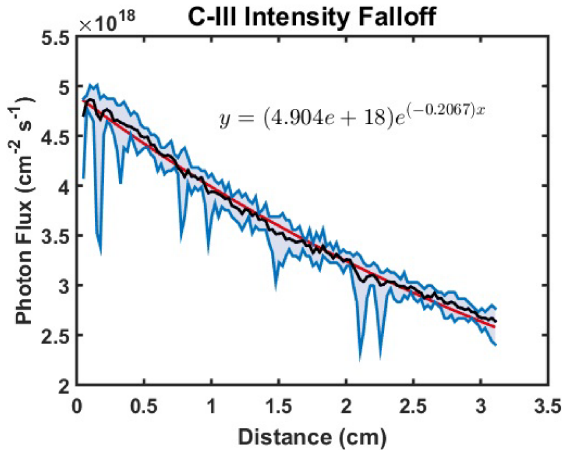

(b)

FIG. 6. (a) One shot of C-III limiter photon flux data with the limiter outline in black. Axes scale in pixels. (b) Mean photon flux data (black line) obtained from averaging the 11 offset, parallel image profiles spanning the blue rectangle. This averaging was done to improve statistics and reduce the effects of CCD noise and mirror dust. The corresponding exponential fit (red line) and the equation of this fit, from which λ_{iz} was determined, are also specified on the plot. The top and bottom of the error regions are taken from the max and min values at each position along the 11 profiles, respectively.

measurement system is not feasible. Assuming a plasma density of 5×10^{17} m^{-3} and a plasma temperature of 70 eV based on Langmuir probe measurements near the last closed flux surface[4] and using the value of the electron ionization rate coefficient at these temperatures,[12] we obtain a penetration distance λ_{iz} of approximately 6.4 cm for molecular hydrogen using this simplified 1D formulation. This value is on the same order as the value obtained experimentally (~a factor of 2 difference). This difference could stem from several assumptions which are not entirely satisfied, including the fact that both atomic and molecular hydrogen emission are contributing to the measured decay length (rather than just molecular hydrogen), the edge temperature and densities are not constant, and therefore the rate coefficient is also not constant. It should be noted that this process is more complex for determining the penetration length of intermediate charge states of carbon; calculating λ_{iz} for C-III would require a collisional radiative model treatment which is beyond the scope of this work.

V. SUMMARY

A limiter-viewing camera system was desired for HSX to investigate 3D stellarator edge physics. Due to the complexities associated with the 3D HSX geometry, obtaining a roughly perpendicular view of the limiter face required an optical system consisting of a mirror and several lenses to be inserted into the HSX edge. This new structure keeps the optical system at the required angle while still allowing the system to be inserted and retracted. Using this system with an absolutely calibrated filtered camera, hydrogen and carbon photon flux images were obtained and analyzed to obtain penetration lengths of 12 ± 1.02 and 4.8 ± 0.3 cm, respectively. This penetration length for hydrogen is within a factor of 2 of a 1D slab estimation of the molecular hydrogen penetration length, which adds some confidence this measurement. Future work will involve converting the photon fluxes to particle fluxes and comparing these data to the magnetic field line calculations and EMC3-EIRENE plasma predictions to obtain more sophisticated edge physics information in this challenging geometry.

ACKNOWLEDGMENTS

This work supported by the US DOE under Grant No. DE-FG02-93ER54222. The authors would also like to gratefully acknowledge O. Schmitz and the TEXTOR team for donating the mirror/lens system that was adapted for this work at HSX.

[1] J. M. Canik, D. T. Anderson, F. S. B. Anderson, K. M. Likin, J. N. Talmadge, and K. Zhai, Phys. Rev. Lett. **98**, 1 (2007).
[2] Y. Feng, F. Sardei, J. Kisslinger, P. Grigull, K. Mccormick, and D. Reiter, Contrib. Plasm. Phys. **44**, 57 (2004).
[3] A. R. Akerson, A. Bader, C. C. Hegna, O. Schmitz, L. A. Stephey, D. T. Anderson, F. S. B. Anderson, and K. M. Likin, Plasma Phys. Controlled Fusion **58**, 084002 (2016).
[4] A. R. Akerson, *Identification of the Helical Scrape-off Layer Structure and Transport Properties in the Edge of HSX*, Ph.D. thesis, University of Wisconsin-Madison, 2016.
[5] I. Shesterikov, Y. Xu, C. Hidalgo, M. Berte, P. Dumortier, M. V. Schoor, M. Vergote, and G. Van Oost, Nucl. Fusion **52**, 042004 (2012).
[6] I. Shesterikov, Y. Xu, M. Berte, P. Dumortier, M. Van Schoor, M. Vergote, B. Schweer, and G. Van Oost, Rev. Sci. Instrum. **84**, 053501 (2013).
[7] A. Pospieszczyk, in *Atomic and Plasma-Material Interaction Process in Controlled Thermonuclear Fusion*, edited by R. Janev and H. Drawin (Elsevier, Amsterdam, 1993), pp. 213–242.
[8] E. Hintz and P. Bogen, J. Nucl. Mater. **128-129**, 229 (1984).
[9] S. Brezinsek, A. Huber, S. Jachmich, A. Pospieszczyk, B. Schweer, and G. Sergienko, Fusion Sci. Technol. **47**, 209 (2005).
[10] P. Stangeby, *The Plasma Boundary of Magnetic Fusion Devices* (Institute of Physics Publishing, 2000).
[11] J. M. Canik, D. T. Anderson, F. S. B. Anderson, C. Clark, K. M. Likin, J. N. Talmadge, and K. Zhai, Phys. Plasmas **14**, 056107 (2007).
[12] R. Freeman and E. Jones, *Atomic Collision Processes in Plasma Physics Experiments*, Technical Report CLM-R–137, 1974.